 doi:10.20944/preprints201910.0222.v1

Article

Thermal and Mechanical Characterization of Copolymer Structure with Gradient Foam Using Additive Manufacturing and CO_2 Foaming

Byung Kyu Park[1,*], Charn-Jung Kim[2], Dong Eui Kwon[3], and Youn-Woo Lee[3,*]

[1] Research Institute of Advanced Materials, Seoul National University, Seoul 151-744, Republic of Korea; bkpark@snu.ac.kr;
[2] School of Mechanical and Aerospace Engineering, Seoul National University, Seoul 151-744, Republic of Korea; kimcj@snu.ac.kr;
[3] School of Chemical and Biological Engineering and Institute of Chemical Processes, Seoul National University, Seoul 151-744, Republic of Korea; ywlee@snu.ac.kr;
* Correspondence: bkpark@snu.ac.kr, (B.K. Park); Tel.: +82-10-3404-7367; ywlee@snu.ac.kr (Y.-W. Lee).

Abstract:

Synthetic polymer-based gradient foams have considered as promising category of functionally graded materials with unique properties. In this study, the carbon dioxide (CO_2) foaming technology has used for PET-PEN (Polyethylene Terephthalate - Polyethylene Naphthalate) copolymer towards porous functional materials with thermal insulation with reasonable mechanical strength. Through scanning electron microscope based morphological characterization, a potential to fabricate gradient foam structures with micro-pores has identified. It has shown that variation of post-foaming temperature can tune the pore size distribution although the very high post-foaming temperature tends to cause structural instability. Thermal measurement data set the limits of operation, confirmed by simultaneous differential scanning calorimeter and thermo-gravimetric analysis. Mechanical stress and thermal conductivity also has measured to find rationale of thermal insulation with reasonable mechanical strength and to elucidate the actual 3D grid foam of copolymer.

Keywords: 3D structure; gradient foam; additive manufacturing; CO_2 foaming; copolymer

1. Introduction

Material foaming is one type of the process that leads to the lighter materials with other functionalities in cost-effective manner. Particularly carbon dioxide (CO_2) foaming has wide application area of sub- and super-critical fluids, and the use of CO_2 as an environmentally benign foaming agent has been under intense investigation for more than scores [1-6]. The basic foaming methodology involves dissolving CO_2 in polymers at high pressure and then imposing a depressurization to bring about phase separation to induce nucleation and cell growth, ultimately leading to the formation of porous structures. Foam properties depend on the thermodynamics of CO_2-solubility in polymers, dictated by pressure and temperature, the kinetics and mechanisms of phase separation, and the dynamics of the CO_2-dependent changes by the thermo-physical and rheological properties of the polymers involved.

Interestingly the idea of polymeric foam was initially developed by MIT group[3] as a means to reduce the amount and costs of plastic polystyrene used to produce a part of products, and since then lots of research and development have done. To name a few, a semi-empirical model for the unfoamed skin thickness on microcellular foams in a plane sheet had suggested [4]. Synthetic polymer-based gradient foams have been considered as promising category of functionally graded

 doi:10.20944/preprints201910.0222.v1

materials due to their unique properties. Composition gradients in polymers have been created by adding filler particles or by adjusting viscosity [5,7]. Thermoplastic foams can serve as lightweight materials with desirable mechanical and thermal properties, and flexibility for wide range of applications [8-14] including thermal insulation materials with proper mechanical properties to maintain the shape when external forces are applied. There have been growing activities on foaming of glassy or semi-crystalline polymers with https://www.preprints.org/manuscript/201910.0221/v1CO_2 for the formation of porous structures such as membranes via phase inversion [15], or multiscale nano-porous structures for insulation applications [16, 17]. Rapid prototyping or additive manufacturing technology has developed and shown advantages in three-dimensional complex structure, especially objects with high surface area, mesh, and cavity, compared with injection molding products. Recently, PET-PEN copolymer has developed as an environmentally benign material, for kitchen and decoration applications among others. Nano-cellular foaming has investigated via supercritical CO_2 as a blowing agent for a few copolymer materials [18].

In this study, we attempt foaming of PET-PEN copolymer materials with carbon dioxide towards fabrication of porous structures with low thermal conductivity and reasonably high mechanical strength, for instances, alternative core material in vacuum insulation panels and scaffolds. The purpose of this paper is providing some data for simple three-dimensional member with gradient foam, which is one of an idealized geometric element in 3-D printed structures. These will contribute to help understanding the behavior of 3D structure solid polymer covered with foams, which has useful functionality and flexibility in design and applications. That is, the results are not only useful for basic level of study on sorption and foaming behavior but also provide guidelines on the 3D printing and subsequent foaming parameters.

2. Experimental apparatus and method

2.1 Material and foaming process

While the ultimate goal of current study is to fabricate arbitrary three-dimensional structures (i.e. freeform) with controlled thermal and mechanical properties by 3D printing combined with CO_2 foaming process [16], the CO_2 foaming process has been separately tested mainly using the base filaments for 3D printing. The radius of cylindrical filament is usually around 0.875 mm, larger than the depths of CO_2 sorption and foaming under current experimental conditions. Therefore, the filaments, as semi-infinite like material platforms, are not only useful for basic level study on sorption/foaming behavior but also provides guidelines on the 3D printing parameters; e.g. unit thickness of 3D printed freeform referring to the sorption/foaming penetration depths. In this study, we examine CO_2 foaming based on PET-PEN (9:1) copolymer filaments of 0.875 mm radius (Kolon Plastics, Kimchun, Korea, true density of 1.33 g/cm^3) as a nontoxic and environmentally friendly material. Selection of copolymer material also has motivated by the possibility of nano-foaming process [17].

Detailed foaming procedures has found from the previous publications [6, 16]. Briefly, liquid CO_2 maintained at 5 MPa and 20 ℃ was fed into a pressure vessel containing samples, and compressed to 10 MPa. Then, the pressure vessel has immersed into cold ethanol/water bath maintained at the temperature of −20 ℃ while maintaining the pressure at 10 MPa during sorption process by continuously pumping under automatic pressure regulation. Various sorption times were applied from 4 to 336 hours to trace the sorption kinetics. After the pressure vessel was depressurized quickly at a pressure drop rate of ~ 100 MPa/s, samples were taken out from the vessel and immersed into a water bath set at designated foaming temperatures of T_f for 3 minutes, followed by quenching in ethanol/water mixture of −20 ℃ for 1 minute to freeze any further cell (pore) growth. The post-foaming temperature, T_f, has varied from 20 to 100 ℃ to seek for its dependence on foaming trend. Finally, samples have wiped out to remove the residual ethanol/water mixture and dried at room temperature. A gravimetric method [19] has used to measure the sorption kinetics and the amount of

CO2 absorbed; weighed on a scale (EPG214, OHAUS, Pine Brook, NJ, USA) before and after each sorption process.

2.2 Measurements

In order to understand the resulting cross-sectional structure, samples have cut at low temperature using liquid nitrogen, and the cut surface was sputter-coated with platinum of ~15 nm thickness. Then, the samples were observed with a field emission scanning electron microscope (FE-SEM, SUPRA 55VP model) with typical acceleration voltage of 2.0 kV. The bulk density, ρ_{foam}, was measured by the weight displacement method [19]. The samples were first weighed on an analytical scale (EPG 214, Ohaus), and volume of water displaced by the sample was then measured. The relative density, ρ_r, can be calculated using the following formula;

$$\rho_r = \frac{\rho_{foam}}{\rho_s}, \quad (1)$$

where ρ_s denotes the density of solid PEN-PET copolymer(1.33 g/cm^3). The cell (pore) nucleation density, N_0, i.e., the number of cells (pores) per unit volume of the foam, and void volume fraction, V_f, can be estimated from the following correlations;

$$N_0 = \left(\frac{nM^2}{A}\right)^{3/2}\left(\frac{\rho_s}{\rho_{foam}}\right), \quad (2)$$

where n is number of cells (pores) in the probe volume, A is probe area, and M is magnification.

For thermal characterization, two-cycle test have performed for as-foamed samples using differential scanning calorimetry (Model Discovery, TA Instrument) based on the ASTM standard (D3417-83, D3418-82). In order to investigate further the weight ratio of organic components contained and the thermal stability at high temperature, the degree of thermal decomposition has measured with a SDT analyzer (simultaneous differential scanning calorimeter and thermo-gravimetric analysis, Universal V4.5A model, TA Instruments). The derivative weights of specimens have measured for the temperature range of 30 – 600 ℃ with heating rate of 10 ℃/min under nitrogen atmosphere. In order to estimate a degree of crystallinity, following equation has used.

$$\text{Degree of Crystallinity} = (\Delta H_m - \Delta H_c)/\Delta H_{m,max}, \quad (3)$$

where ΔH_m is the measured heat of fusion and ΔH_c is the heat of crystallization. Assuming an enthalpy of fusion 140.0 J/g for a 100% crystalline PET-PEN copolymers with infinite crystal thickness (i.e. $\Delta H_{m,max}$ = 140.0 J/g taken here).

Compressive tests has carried out to evaluate the mechanical properties of the fabricated structures. For the mechanical strength measurement, a universal material testing machine (UTM, LR 50K model, LLOYD Instruments, West Sussex, UK) was used, and at least four specimens were prepared for each experimental group. The crosshead speed was set based on the ASTM standard (ASTM D695).

Thermal conductivity has measured to estimate the thermal insulation performance. For the thermal property measurements, the transient plane source method (Hot Disk Thermal Constants Analyzer, TPS3500, Göteborg, Sweden), based on ISO standard (ISO 22007-2:2015), was used for four combination arrangements of two equivalent specimens prepared.

Preprints (www.preprints.org) | NOT PEER-REVIEWED | Posted: 19 October 2019 doi:10.20944/preprints201910.0222.v1

3. Results and discussion

3.1 Sorption kinetics and microstructural characteristics

Sorption tests have conducted to find the saturation time of the PET-PEN filament. Even though there are argues, the sorption of carbon dioxide into polymer has assumed to follow corresponding Fick's law. Then, the "pseudo" diffusion coefficient and saturation concentration can be estimated approximately from the CO_2 concentration values experimentally measured as function of time, based on the following solution of diffusion equation [20];

$$\frac{C_t}{C_{sat}} = 1-\sum_{n=1}^{\infty}\frac{4}{\alpha_n^2 a^2}\exp(-D\alpha_n^2 t), \quad (4)$$

where C is CO_2 concentration (the ratio between mass of CO_2, and copolymer filament measured), a is the radius of cylindrical rod, $J_o(x)$ is the Bessel function of the first kind of order zero, and α_ns are the eigenvalues, that is, the roots of $J_o(a\alpha_n)=0$. C_t and C_{sat} denote the concentration of diffusing substance (CO_2) entering the cylinder in time t and after infinite time, respectively.

Figure 1 shows the sorption behavior of CO_2 in PET-PEN copolymer filaments at 10 MPa as function of time in order to confirm the partial sorption and degree of saturation. As expected, the CO_2 concentration steeply increased initially, and gradually converged to a saturation concentration. The measured data are well fitted to Equation (4), and the estimated CO_2 uptake and charging diffusivity at −20°C are C_{sat} = 73.31 mg(CO_2)/g(copolymer) and D = 1.095 × 10^{-9} cm^2/s, respectively at the confidence level of 95%. It has also found that the estimated saturation time is around 20 days. Since practically it takes too long to reach a saturation state, further parametric studies have based on partial sorption process by a fixed time of 24 hours. In turn, it facilitated the formation of gradient foam in PET-PEN copolymer, as will be explained.

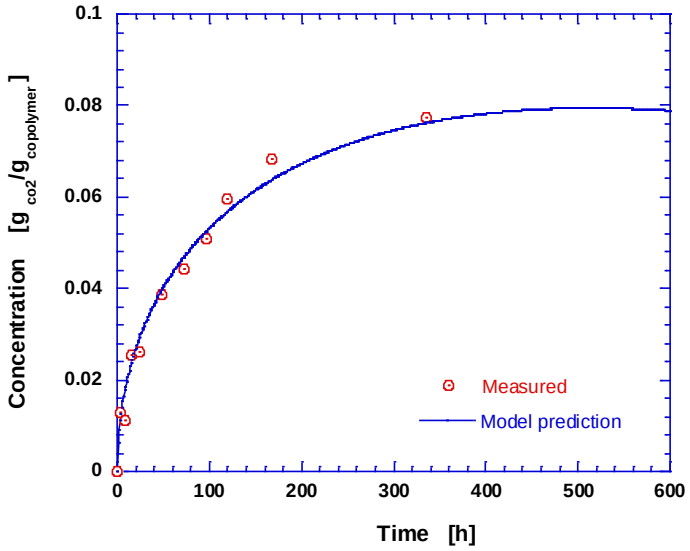

Figure 1 CO_2 Sorption kinetics in PET-PEN copolymer.

Figures 2 show typical photographs before and after the post-foaming of typical 3-D printed structures. Figures 2 (a) and (b) are for bottom views of samples, and Figures (b) and (d) are top views, respectively. It shows simple regular three-dimensional structures with well-arranged members (ribs) while the post-foaming did not noticeably alter overall feature characteristics for T_f = 60 ℃.

 doi:10.20944/preprints201910.0222.v1

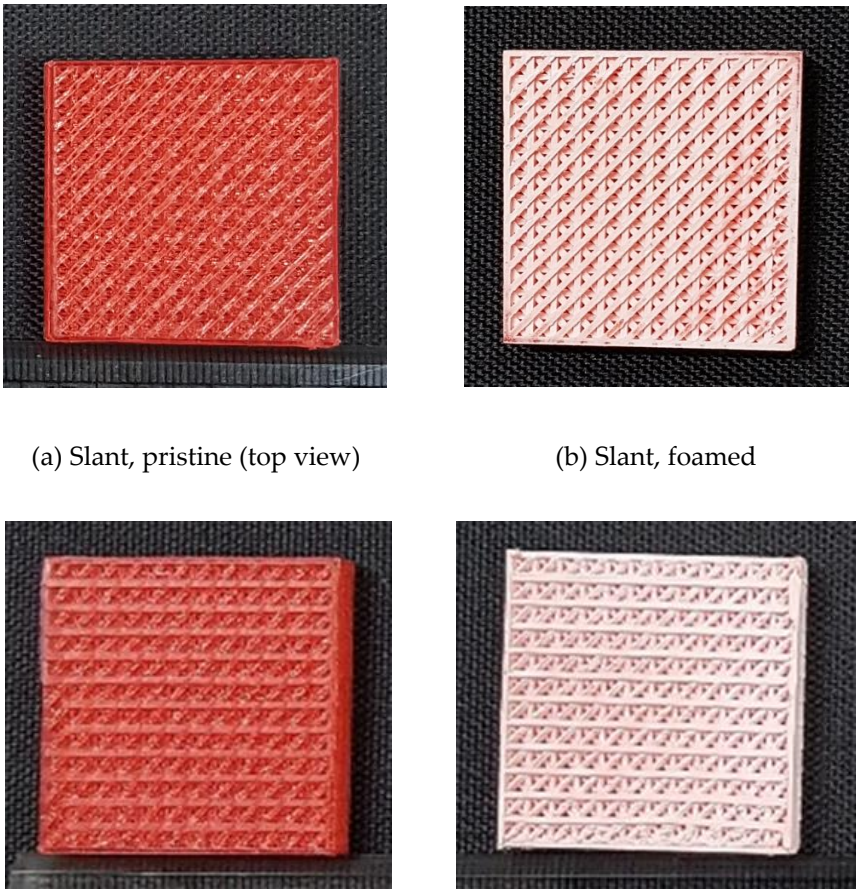

(a) Slant, pristine (top view) (b) Slant, foamed

(c) Horizontal, pristine (bottom view) (d) Horizontal, foamed

Figure 2 Typical 3D freeform structure as printed (a,c) and post-foamed (b,d).

Figure 3 shows the cross sectional SEM images for cylindrical rod and rib of 3D gird. The overall configuration of actual foamed 3D grid in the inset is very complex compared to that of cylindrical rod. However, the zoomed-in images for the foamed region show more detail shapes. Note that there are similar morphology in the SEM images shown and resulting features of gradient foam excepting for curvature. Therefore, as a fundamental investigation of the gradient foam, we have assumed that the filament of cylindrical rod as a simply idealized substitute object for actual rib member inside 3D printed structure. It is seen that partial CO_2 sorption under current experimental conditions induced gradient foaming along radial direction of PET-PEN copolymer filaments. In general, the penetration depth in partial sorption will depend on the pressure, temperature, and sorption time. After a quick pressure relief, the CO_2 in the saturated sample becomes unstable and tends to foam. Thus, the concentration gradient can induce a foam gradient. The CO_2 concentration at the filament surface will be quite high just before depressurization. However, on depressurizing, it decrease rapidly in the outer region and the temperature of environmental gas surrounding polymer will change due to the Joule-Thomson effect (temperature reduction that accompanies depressurization). It causes reduction in viscosity as CO_2 leaves the copolymer matrix, making the diffusion process will be suppressed. On the contrary, the residual CO_2 in the penetration depth of filaments is diffusing to equalized, and the subsequent post-foaming process make distribution of gradual pore sizes. Finally, the cells of gradient foam has obtained through the interactions of many parameters. In short, It is assumed that the gradient foaming characteristics, e.g., foaming depth and pore size distribution in Figure 3(a), achieved in the filament rod are represented in the 3D printed structures shown in Figure 3(b), and

Preprints (www.preprints.org) | NOT PEER-REVIEWED | Posted: 19 October 2019 doi:10.20944/preprints201910.0222.v1

can be applied with correction parameters in design of arbitrary freeform foam by 3D printing and CO_2 foaming processes.

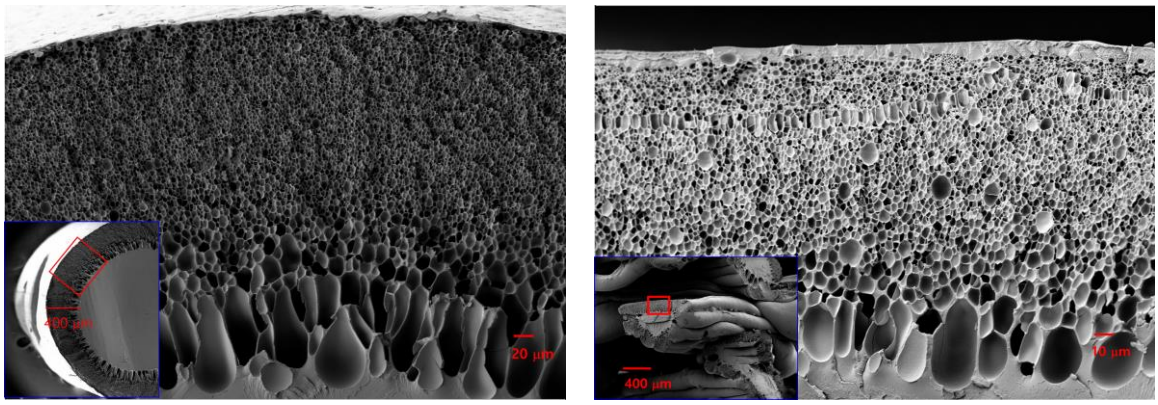

(a) Filament rod (b) Rib of 3D printed grid

Figure 3 SEM micrographs of the foamed PET-PEN copolymer. Results are for filament rod (a) and additively manufactured grid structure (b).

In order to find further the characteristics of foams, the pore size distribution has measured from the SEM images and analyzed using the ImageJ (NIH) and MorphoLibJ package libraries. The effective pore diameters were calculated from the measured cross-sectional areas, based on the formula, $d_{pore} = \sqrt{(4A/\pi)}$, assuming circular pores, where A is the cross-sectional area, and d_{pore} is the effective diameter.

The effects of post-foaming temperature on the pore characterization are represented in Figure 4. The cell nucleation density ρ_r gradually increases up to the post-foaming temperature of 80 ℃, but abruptly increases at 100 ℃ that is higher than the glass transition temperature of PET-PEN copolymer. The number-averaged diameter, d_{pore}, obtained from image analysis increase very slowly as 3.08 μm, 3.12 μm, 3.99 μm, 4.57 μm, 5.26 μm respectively as T_f increase from 20 ℃, 40 ℃, 60 ℃, 80 ℃, to 100 ℃ respectively. Although the pore size distributions have estimated from SEM images, we also confirmed negligible fraction of sub-micron pores from further zoomed-in SEM images. The relative density ρ_r gradually reduced up to the post-foaming temperature of 80 ℃, but largely decreased at 100 ℃ due to asymmetric big pores near the inner boundary (not shown).

Preprints (www.preprints.org) | NOT PEER-REVIEWED | Posted: 19 October 2019 doi:10.20944/preprints201910.0222.v1

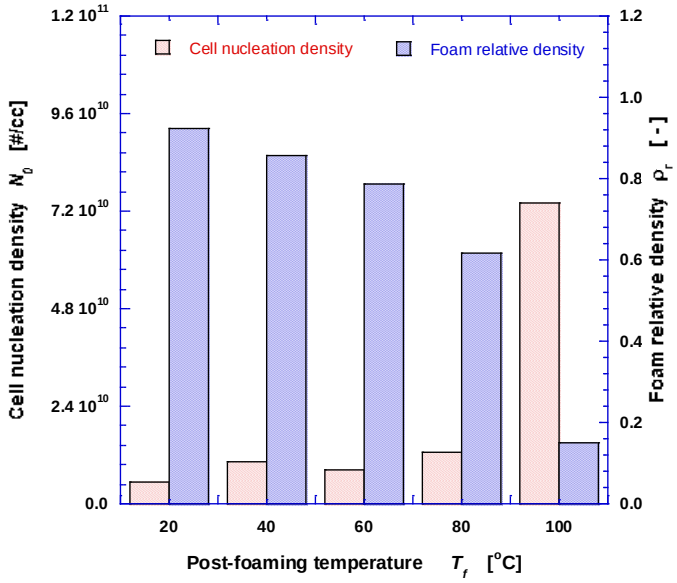

Figure 4 Effect of post-foaming temperature on (a) cell nucleation density (left) and relative density (right) for PET-PEN cylindrical filaments (sorption at 10 MPa and -20 ℃ for 24 hours).

3.2 Calorimetric and Pyrolysis Analyses

Thermal analyses have performed for both raw rod and foamed grid structure as shown in the left of Figure 5(a) (temperature range from 34 up to 300°C). Two-cycle tests were conducted to investigate the detailed states of PET-PEN copolymer, i.e., for experimental measurements of glass transition temperatures for the first and second cycles using differential scanning calorimetry. The analysis has carried out in an aluminum container in a nitrogen. The sample of 3 - 5 mg in weight has used. The samples were first heated up from 34 to 300°C at the ramping rate of 5°C/min, held at 300°C for 60 minutes, and cooled down to 34°C at the same rate of 5°C/min, completing the first cycle, and then the second cycle was repeated in an identical manner after sufficiently stabilized condition.

During heating of the raw sample, as seen from Figure 5(a), the initial phase transition took place at 75.9°C, which corresponds to the glass transition temperature in which the polymer transitions to a highly elastic state. The endothermic peak at 241.4°C indicates crystalline melting process. Observation of thermal transitions at temperature peaks of 140.5°C is associated with cold crystallization. Cold crystallization has caused by the rearrangement of molecular chains in the crystalline PET-PEN layer assisted by increased mobility during the manufacturing and heating processes. Since the polymer was in an amorphous state after the heating stage, such phase transition was present. During the cooling process (not shown) in the first cycle, exothermic energy of 33.1 J/g, with the peak center at 169.5°C was due to cooling crystallization of PET-PEN. From the thermograms the first and second exothermic peak energies are obtained as 3.56 J/g and 32.17 J/g, respectively. The degree of crystallinity has increased from 2.5 to 23 %. However, in the second cycle neither the exothermic peak due to cold crystallization nor double melting peaks, appeared eminently in PLA and made possible the innovative bead foam, were shown [12]. On the other hand, the foamed grid samples with gradient foam show clear difference in the first heating stage in that lower cold crystallization occurred due to rearrangement of molecular chains by the solid state foaming process and lower crystalline peak. By the second heating, for both raw and foamed samples, there were ambiguous glass transitions and negligible cold crystallizations.

Preprints (www.preprints.org) | NOT PEER-REVIEWED | Posted: 19 October 2019 doi:10.20944/preprints201910.0222.v1

Pyrolysis measurements have performed using a SDT (simultaneous DSC / TGA) analyzer for non-foamed raw filament rod and foamed 3D grid structure. As observed from the pyrolysis curve, Figure 5(b), obtained by thermo-gravimetric analysis (TGA), the PET-PEN copolymer starts to evaporate near 360 ℃ and has maximum weight loss rate at 437.1 ℃ (~2.0 wt. %/℃). Major pyrolysis event takes place between 380 - 520 ℃, where most of latent heat of evaporation is consumed. It is noted that for temperature higher than ~380 ℃, thermal decomposition rate of filament material rapidly increases, resulting in a large mass loss, and thus the upper limit of working temperature for 3D printed features based on PET-PEN filament should be set sufficiently lower than 300 ℃. There is also not significant differences between raw rod and foamed grid structure except for initial melting.

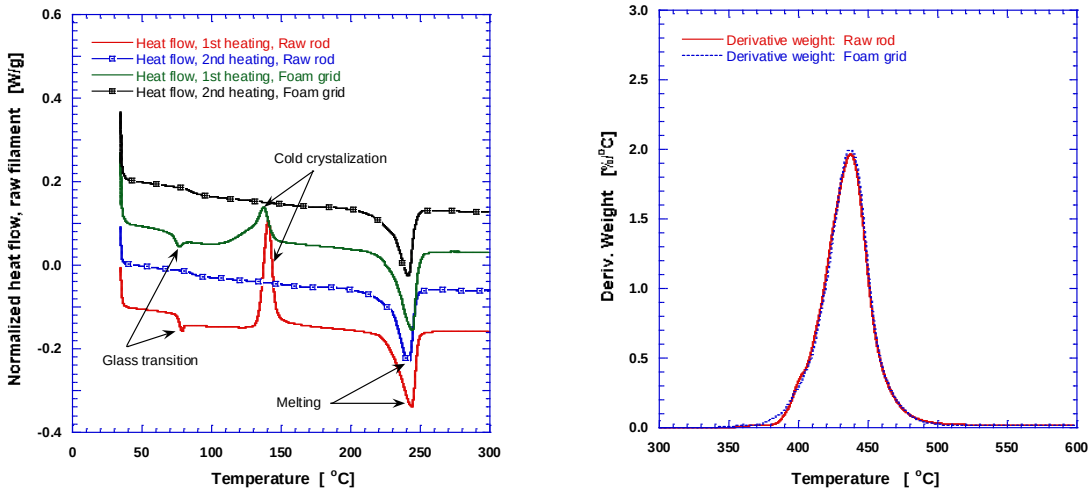

(a) (b)

Figure 5 (a) DSC and (b) TGA thermograms of the PET-PEN specimens for raw rod and foamed grid structure.

3.3 Mechanical Compressive Stress

To understand the mechanical properties of 3D structures fabricated by 3D printing and CO_2 foaming technologies, representative compressive test results are displayed in Figure 6. The main reasons for improved mechanical strength in comparison to typical insulating foams is the 3D printed solid structure of PET-PEN copolymer with crystalline due to soaking inside has a relatively strong bonding force between melt-bonding layers. The dimension of pristine specimen before compression test was 36.0 × 36.0 × 5.4 mm^3. The maximum compressive deflection was limited to ~4.0 mm for the protection of measuring equipment with overload protection during compression. In compressive test, freeform specimens showed linear elastic behavior for the compressive strain range of ~0.04–0.12 mm/mm and flat region for the strain range of 0.22–0.40 mm/mm with nearly constant compressive stress. In the compression, the specimen did not rupture rapidly until strain reached about 40% because the space between inner solid grids in polymer matrix studs and surrounding gradient foams can accommodate and withstand high strains maintaining the connectivity.

It has observed that the modulus of elasticity increases as the post-foaming temperature increases. The highest mechanical strength of CO_2 saturated grid sample is greater than that of pristine one presumably because crystals have rearranged due to the plasticization effects by CO_2 impregnation. The maximum compressive stress increased by about 13.5%, from 9.20 MPa to 10.44 MPa. And the compressive modulus of elasticity were calculated as 75.06 MPa, 98.56 MPa, 108.09

Preprints (www.preprints.org) | NOT PEER-REVIEWED | Posted: 19 October 2019 doi:10.20944/preprints201910.0222.v1

MPa, 77.87 MPa, 61.55 MPa, 47.09 MPa for the manufactured freeform, soaking, and post-foaming temperature of 20 °C, 40 °C, 60 °C, 80 °C, respectively. It does not found that the formation of nano-scale structure but it may be possible by suitable tuning of foaming conditions. Further basic researches on the controlling mechanisms of the cell size and finding correlation between foaming configuration are under way.

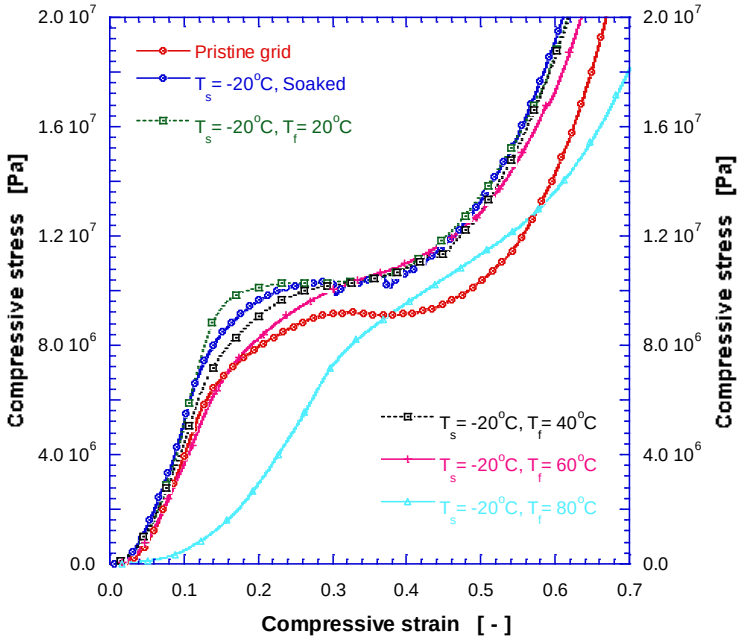

Figure 6. Compressive stress-strain curves for 3D grid structure of PET-PEN copolymer.

3.4 Thermal conductivity

Various thermal insulation systems taking advantage of different types of thermal insulation materials on both an organic and inorganic bases are being designed and tested, and new methods for analyzing the properties of insulation material and system are being devised. In order to increase the thermal performance in this study some voids in insulation system are involved inside and outside of materials. Even though thermal conductivity is a very important property in heat transfer, it is rare for gradient foam. Therefore the data for four combination configurations of two equivalent samples(Figure 2) have measured the transient plane source method [21] and plotted in Figure 7. Even though there are small deviations for different arrangements it has found that thermal conductivity decrease quite slowly as the post-foaming temperature increase and have around 0.06~0.08 W/m·K in the range of this study. The slow decrease in thermal conductivity is considering mainly due to the unfoamed skin thickness. In the post-foaming temperature of 100 ℃, there is a significant decrease in thermal conductivity, due to big pores near the outer edge of central solid copolymer. The effects of average thermal conductivity, thermal diffusivity, and heat capacity on post-foaming temperature have shown in Figure 8. Thermal diffusivity increases with post-foaming temperature, while heat capacity decrease with the temperature.

Preprints (www.preprints.org) | NOT PEER-REVIEWED | Posted: 19 October 2019 doi:10.20944/preprints201910.0222.v1

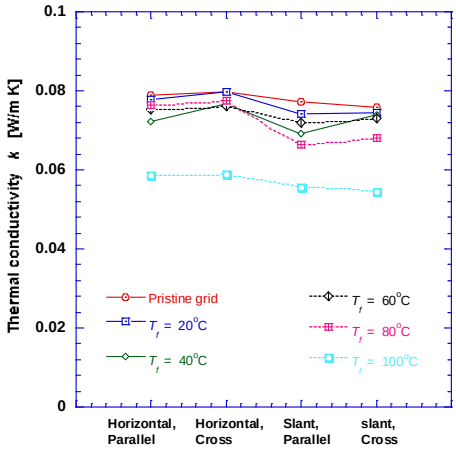

Figure 7. Thermal conductivity for various arrangements in 3D grid foam structure of PET-PEN copolymer.

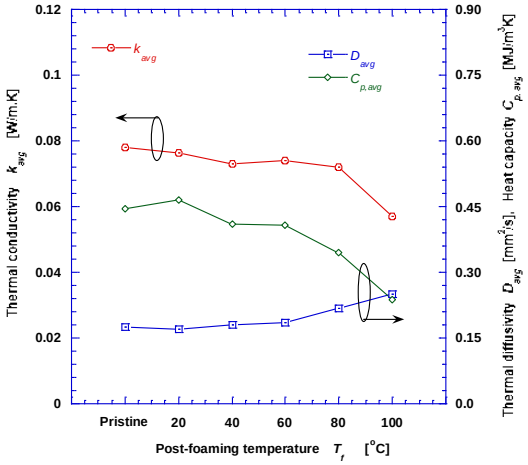

Figure 8. Effects of average thermal conductivity, thermal diffusivity and heat capacity on the post-foaming temperature in 3D grid foam structure of PET-PEN copolymer.

As the post-foaming temperature goes up, the thermal insulation performance has possibly improved by taking advantage of larger volume of foams near the filament core yet at the expense of mechanical strength probably due to weak connectivity between foamed region and the filament core. There should be trade-off depending on specific target applications. Conventionally insulation materials have focused on improving insulation performance, without considering the mechanical strength. However, a moderate compressive strength is required in many applications. The ratio of strength to thermal conductivity (σ/κ) has introduced to indicate a performance index in this study because the thermal conductivity of a material increases in proportion to its density generally. It has shown in Table 1 for several foams. It has confirmed that the performance index in the 3D forming structure was significantly higher than that of other foams.

Table 1 Mechanical and thermal properties for typical polymer foams

 doi:10.20944/preprints201910.0222.v1

Polymeric foam type	σ_c [Mpa]	E [Mpa]	k [W/m.K]	ρ [kg/m^3]	σ_c / k [Mpa.m.K /W]	source
PET foam	1.3		0.033	110	39.39	[22]
SAN foam	1.98		0.04	115	49.5	[22]
PEI foam	1.3		0.04	110	32.5	[22]
PET-PEN, foamed grid	10.44	75.06	0.072	436	143.1	Present
PUR.spray&preform	0.1		0.023	160	4.35	Thermal Insulation HB

4. Conclusions

In this study, a micro-porous structure has fabricated with PET-PEN copolymer by 3D printing and CO_2 foaming technologies. Through morphological investigation, a potential to fabricate macroscale gradient foam structures with micro-pores has identified, having beneficial aspects towards thermal insulation material with reasonable mechanical strength. Variation of post-foaming temperature could tune the pore size distribution, and possibly the post-foaming temperature higher than the glass transition temperature could ameliorate thermal insulation performance while it can deteriorate mechanical strength of 3D structures, implying that trade-offs are needed. Thermal decomposition of filament material set the upper and lower limits of working temperature, as confirmed by simultaneous DSC / TGA analysis. It has found that the compressive stress of CO_2 soaked samples has increased higher than that of pristine. From the measurements using transient plane source method, it has found that the thermal conductivity decrease as the post-foaming temperature increase, having around 0.06~0.08 W/m·K in the range of this study. It has been realized freeform foam structures for good thermal insulation with reasonable mechanical strength. Further study is necessary to elucidate a wider range of gradient foam, double melting peaks, and nano-foaming mechanisms by exploring processing window for copolymer types and compositions.

Acknowledgments (Funding): This research has supported by Grant (NRF-2018R1A2B2008196) from National Research Foundation of Korea funded by Ministry of Science and ICT of Korea government.

Conflicts of Interest: The authors declare no conflict of interest. Authors identify and declare no personal circumstances or interest that may be perceived as inappropriately influencing the representation or interpretation of research results. The funders had no role in the design of the study; in the collection, analyses, or interpretation of data; in the writing of the manuscript, and in the decision to publish the results.

References

1. Maio, E.D.; Kiran, E. Foaming of polymers with supercritical fluids and perspectives on the current knowledge gaps and challenges, J. Supercritical Fluids 2018, 134, 157-166.
2. Ngo, M.T.; Dickmann, J.S.; Hassler, J.C.; Kiran, E. A new experimental system for combinatorial exploration of foaming of polymers in carbon dioxide: The gradient foaming of PMMA, J. Supercritical Fluids 2016, 109, 1-19.
3. Martini J.E.; Waldman F.A.; Suh N.P. The Production and analysis of microcellular thermoplastic foams, SPE Technical Papers, 1982, Vol.28, p.674.
4. Kumar, V.; Weller J.E. A Model for the unfoamed skin on microcellular foams, Polymer Engineering and Science, Vol. 34, 1994, pp 169-173.
5. Yu J.; Song, L.; Chen, F.; Fan P.; Sun, L.; Zhong, M.; Yang, J. Preparation of polymer foams with a gradient of cell size: Further exploring the nucleation effect of porous inorganic materials in polymer foaming, Materials Today Communications, 2016, Vol.9, pp.1–6.

6. Xia, T.; Xi, Z.; Tao Liu, T.; Zhao, L. Solid state foaming of poly(ethylene terephthalate) based on periodical CO2-renewing sorption process, Chemical Engineering Science, 2017, Vol.168, pp.124–136.
7. Zhou, C.; Wang, P.; Li, W. Fabrication of functionally graded porous polymer via supercritical carbon dioxide foaming, Composites: Part B 2011, 42, 318-325.
8. Cao, X.; Dai, X.; Liu, J. Building energy-consumption status worldwide and the state-of-the-art technologies for zero-energy buildings during the past decade, Energy and Buildings, 2016, Vol. 128, Issue 15, pp. 198~213.
9. Jelle, B.P. Traditional, state-of-the-art and future thermal building insulation materials and solutions – Properties, requirements and possibilities, Energy and Buildings, 2011, Vol. 43, Issue 10, pp. 2549~2563.
10. Wang, Z.; Zhang, T.; Park, B.K.; Hwang, D.J. Minimal contact formation between hollow glass microparticles toward low-density and thermally insulating composite materials, J. Mater. Sci., 2017, Vol.52, pp.6726–6740.
11. Noordegraaf, J.; Matthijssen, P.; de Jong J., de Loose P.A., Comparative LCA of building insulation products, Bioplastic Magazine, 2011, Vol.6, pp.30-33.
12. Nofar, M.; Ameli, A.; Park, C.B. Development of polylactide bead foams with double crystal melting peaks, Vol.69, 2015, pp.83-94.
13. Lee, G.H.; Park, B.K.; Lee, W.I. Microstructure and Property Characterization of Flexible Syntactic Foam for Insulation Material via Mold Casting, International Journal of Precision Engineering and Manufacturing-Green Technology, 2017, Vol. 4, pp.169-176.
14. Berro, S.; Ahdab, R.E.; Hassan, H.H.; Khachfe, H.M.; Hassan, M.H. From Plastic to Silicone: The Novelties in Porous Polymer Fabrications, Journal of Nanomaterials, 2015, Vol. 2015, Article ID 142195, 21 pages.
15. Kiran, E. Morphological modifications and formation of morphologically-gradient polymers in dense fluids, Proceedings of the 5th International Symposium on High Pressure Process Technology and Chemical Engineering, Segovia, Spain, 2007, pp. 1–10.
16. Park, B.K.; Hwang, D.J.; Kwon, D.E.; Yoon, T.J.; Lee, Y.-W. Fabrication and Characterization of Multiscale PLA Structures Using Integrated Rapid Prototyping and Gas Foaming Technologies. Nanomaterials 2018, 8, 575.
17. Forest, C.; Chaumont, P.; Cassagnaua, P.; Swoboda, B.; Sonntag, P. Polymer nano-foams for insulating applications prepared from CO2 foaming, Progress in Polymer Science, 2015, Vol.39, pp.1721-1741.
18. Costeux, S. CO2-Blown Nanocellular Foams, J. Applied Polymer Science, 2014, Vol.131, Issue 23, DOI: 10.1002/app.41293.
19. Yoon, T.J.; Kong, W.; Kwon, D.E.; Park, B.K.; Lee, Y.-W. Preparation of solid-state micro- and nanocellular acrylonitrile-butadiene-styrene (ABS) foams using sub- and supercritical CO2 as blowing agents, J. of Supercritical Fluids 2017, 124, 30-37.
20. Crank, J. The mathematics of diffusion, second ed. Oxford university press, 1975.
21. ISO 22007-2:2015, Plastics - Determination of thermal conductivity and thermal diffusivity - Part 2: Transient plane heat source (hot disc) method.
22. Lee, S.T.; Polymeric foams : Innovations in process, technologies and products, 2017, CRC press.